

Kinetically Locked-In Colloidal Transport in an Array of Optical Tweezers

Pamela T. Korda, Michael B. Taylor,* and David G. Grier

Department of Physics, James Franck Institute and Institute for Biophysical Dynamics, The University of Chicago, Chicago, Illinois 60637

(Received 8 January 2002; published 3 September 2002)

We describe measurements of colloidal transport through arrays of micrometer-scale potential wells created with holographic optical tweezers. Varying the orientation of the trap array relative to the external driving force results in a hierarchy of lock-in transitions analogous to symmetry-selecting processes in a wide variety of systems. Focusing on colloid as a model system provides the first opportunity to observe the microscopic mechanisms of kinetic lock-in transitions and reveals a new class of statistically locked-in states. This particular realization also has immediate applications for continuously fractionating particles, biological cells, and macromolecules.

DOI: 10.1103/PhysRevLett.89.128301

PACS numbers: 82.70.Dd, 05.45.-a, 42.40.-i

Depending on the balance of forces, a particle driven across a corrugated potential energy landscape either flows with the driving force or else becomes locked-in to a symmetry-preferred route through the landscape. The emergence of kinetically locked-in states whose transport properties are invariant over a range of control parameters characterizes many systems and is referred to variously as phase-locking, mode-locking, and stochastic resonance. Examples arise in the electromigration of atoms on crystal surfaces [1], in flux creep through type-II superconductors [2,3], in flux tunneling through Josephson junction arrays [4], and in electron transport through charge density waves and two-dimensional electron gases [5]. Related problems abound in the theory of chemical kinetics and glass formation.

Despite their ubiquity, kinetically locked-in states and transitions among them have been observed directly only in numerical simulations. Their presence in experiments has been inferred indirectly from their influence on collective large-scale properties such as the magnetoresistance and Hall conductance of superconductors and two-dimensional electron gases. Consequently, most theoretical studies have addressed the collective transport properties of strongly coupled systems whose internal interactions modify the influence of the modulated potential and the external driving force. How kinetic lock-in affects single-particle transport has received far less attention.

This Letter describes observations of a hierarchy of kinetically locked-in states in the microscopic trajectories of individual colloidal particles flowing classically through large arrays of optical tweezers. Unlike previous studies on other systems which have found that locked-in states correspond to deterministically commensurate trajectories through the potential energy landscape, our observations also reveal a new class of statistically locked-in states. The locked-in states' ability to systematically and selectively deflect particles' trajectories suggests that optical trap arrays will be useful for continuously fractionating materials in suspension.

Previous studies [6] have created optical potential energy landscapes with static interference patterns and studied their influence on the equilibrium phase behavior of strongly interacting colloidal monolayers. The present study extends this approach to explore colloidal kinetics in adjustable arrays of discrete potential wells.

Our system, shown schematically in Fig. 1, consists of colloidal silica spheres $2a = 1.5 \mu\text{m}$ in diameter (Bangs Labs Lot 4258) dispersed in a $20 \mu\text{m}$ -thick layer of deionized water sandwiched between horizontal glass surfaces. These spheres are considerably denser than water and readily sediment into a monolayer about $1 \mu\text{m}$ above the lower wall [7]. The edges of the sample volume are sealed to form a flow cell, with access provided by two glass tubes bonded to holes passing through the upper glass wall. These tubes also serve as reservoirs for colloid, water, and clean mixed-bed ion exchange

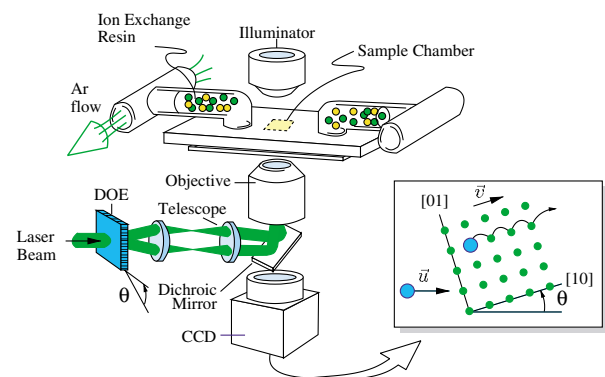


FIG. 1 (color online). Schematic diagram of the experimental system. Laser beams formed by a diffractive optical element (DOE) are transferred by a telescope to the input pupil of a high-NA objective lens which focuses each into an optical trap. The same lens is used in a conventional light microscopy system (illuminator, condenser, objective, video eyepiece, and CCD camera) to form images of spheres moving past the traps, as shown schematically in the inset. A spatial filter blocking the undiffracted laser light is omitted for clarity.

resin. Their ends are connected to continuous streams of humidified Ar gas which minimize the infiltration of airborne contaminants and enable us to drive the colloid back and forth through the channel. Blocking one of the gas streams causes a pressure imbalance which forces the dispersion through the sample chamber and past the $75 \times 58 \mu\text{m}^2$ field of view of a $100\times$ numerical aperture (NA) 1.4 oil-immersion objective mounted on an Olympus IMT-2 microscope base. Steady flows of up to $u = 100 \mu\text{m/s}$ can be sustained in this way for about 10 min.

We use precision digital video microscopy [8] to track the individual spheres' in-plane motion with a resolution of 10 nm at $1/60$ s intervals. The resulting trajectory data allow us to monitor the spheres' progress through potential energy landscapes that we create with light.

Our optical potential landscapes are created with the holographic optical tweezer technique [9,10] in which a single beam of light is formed into arbitrary configurations of optical traps by a computer-designed diffractive beam splitter. Each beam created by the diffractive optical element (DOE) is focused by the objective lens into a diffraction-limited spot which acts as an optical tweezer [11] capable of stably trapping one of the silica spheres against gravity and random thermal forces. For the present experiments, we created a planar 10×10 array of optical traps on $2.4 \mu\text{m}$ centers using light from a frequency-doubled Nd : YVO₄ laser operating at 532 nm. The traps are focused into the plane of the monolayer to avoid displacing spheres vertically as they flow past. Each trap is powered by about $150 \mu\text{W}$, and their intensities vary by $\pm 20\%$ from the mean, as determined by imaging photometry. Rotating the DOE through an angle θ , as shown in Fig. 1, rotates the array of traps relative to the flow, \vec{u} , by the same amount, without otherwise affecting the traps' properties [10].

If the Stokes drag due to the flowing fluid greatly exceeds the optical tweezers' maximum trapping force, then colloidal particles flow past the array with their trajectories unperturbed. Conversely, if the trapping force dominates, then particles fall irreversibly into the first traps they encounter. Our observations are made under intermediate conditions for which trapping and viscous drag are nearly matched and particles hop readily from trap to trap. Our silica spheres enter the hopping state for flow speeds u in the range $40 \mu\text{m/s} < u < 80 \mu\text{m/s}$. The monolayer's areal density is low enough that typically only one or two spheres are in the array at any time. Their separations are large enough that hydrodynamic coupling between spheres should be negligible [12].

Figure 2 shows the superimposed trajectories of 300 particles flowing through a $9 \times 9 \mu\text{m}^2$ section of the field of view which includes one corner of the optical tweezer array. The flow drives spheres directly from left to right across the field of view, with small lateral deviations resulting from Brownian fluctuations. Those spheres passing within about $1.5 \mu\text{m}$ of the optical traps are drawn into the array's [10] rows and follow them to their ends. In

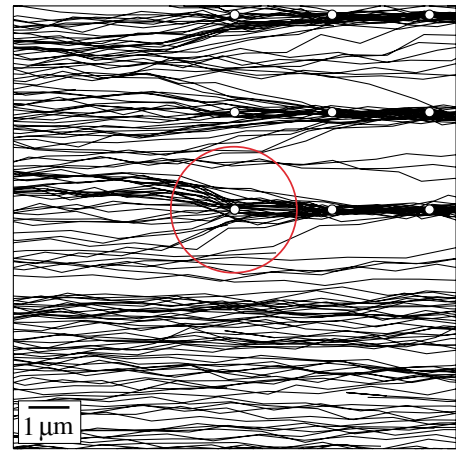


FIG. 2 (color online). Spheres flowing through an array of optical traps follow channels along the [10] direction of the trap lattice. White spots denote tweezer positions, and the $3 \mu\text{m}$ -diameter circle indicates an individual tweezer's region of influence. Traces show the paths of 300 separate spheres tracked in $1/30$ s intervals over a 3 min period.

this case, the [10] rows are aligned with the bulk flow, and the traps' principal influence is to herd particles into well-defined channels and to suppress their transverse fluctuations. The appearance of such commensurate trajectories through the array defines a channeling state, named by analogy to ion channeling through conventional crystals.

While plotted trajectories help to visualize individual particles' interactions with the optical traps, a complementary view of the array's overall influence is offered by the relative probability $P(\vec{r}) d^2r$ of finding a particle within d^2r of \vec{r} at some time after it enters the field of view. Figure 3(a) shows data compiled from the trajectories of 18 601 spheres obtained under the same conditions as Fig. 2. They reveal that spheres are nearly 7 times more likely to be found in the rows of traps than at any point in the bulk flow outside of the array. The correspondingly low probability for finding spheres between the rows and the comparatively subtle modulation along the rows reveals that the time required for a sphere to hop from trap to trap along a row is so much shorter than the time needed for a transverse jump that the spheres essentially never leave the [10] rows. Once the spheres have hopped through the ranks of traps, they return to the bulk flow, their trajectories eventually blurring into each other through diffusion.

Figure 3(b) shows data from the same sample but with the traps oriented at $\theta = 9^\circ$ with respect to the flow. Even though the flow is no longer aligned with the lattice, the spheres still closely follow the array's [10] rows. As a result, the channeling trajectories are systematically deflected away from the flow's direction and leave a distinct shadow downstream of the array. This insensitivity to orientation distinguishes the [10]-commensurate state as being kinetically locked-in and confirms the conjecture [2,5] that kinetic lock-in with systematic deflection can

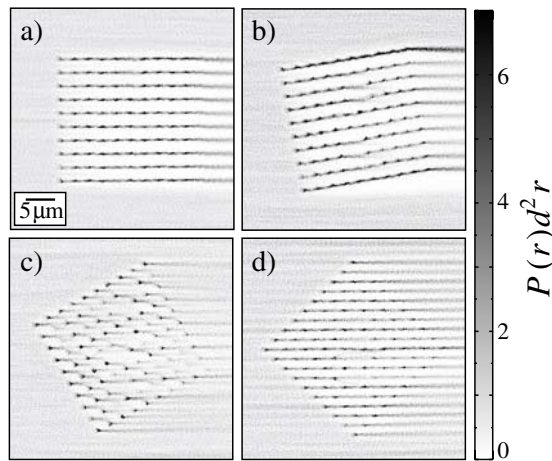


FIG. 3. Relative probability that a sphere will pass through a point in the field of view, when the $[10]$ direction of the trap lattice is oriented at (a) $\theta = 0^\circ$, (b) 9° , (c) 28° , and (d) 45° . In all figures, the external flow is from left to right.

occur as a single-body process rather than requiring the elasticity of an interacting monolayer.

When the trap array is rotated even further to $\theta = 28^\circ$, as in Fig. 3(c), the particles no longer channel along the $[10]$ direction. Although the spheres still spend more time in individual traps than in the bulk, they no longer follow clearly defined paths from one trap to another.

Rotating to $\theta = 45^\circ$, as in Fig. 3(d), reveals another channeling state with particles following the array's diagonal $[1\bar{1}]$ rows. Rotating away from 45° demonstrates this channeling state also to be locked-in. In principle, additional locked-in channeling states should appear at other angles corresponding to commensurate paths through the array [13]. In a system with square symmetry, commensurate orientations occur for rational values of $\tan\theta$.

To quantify the degree to which the array deflects spheres' trajectories, we compare the velocity \vec{v} a particle attains while moving inside the array to its velocity \vec{u} in the bulk flow. In particular, Fig. 4(a) shows the mean normalized transverse component of the in-array velocity $v_\perp(\theta)/u = [\vec{v}(\theta) \times \vec{u}]/(uv)$ which is roughly analogous to the Hall coefficient in electron transport. The monotonically positive slope of $v_\perp(\theta)/u$ in the range $|\tan\theta| < 0.2$ characterizes the domain over which the $[10]$ state is locked-in, with increasing rotation yielding systematically increasing deflection.

After the deflection reaches its maximum at $\tan\theta = 0.2$, it decreases nonmonotonically to zero at the commensurate orientation $\tan\theta = 1/2$. Rotating the array beyond this point results in *retrograde* deflection. In contrast, no change of sign is predicted for the Hall coefficient of a periodically modulated two-dimensional electron gas with increasing magnetic field, although this may reflect the choice of sixfold rather than fourfold symmetry for the potential landscape in the available simulations [5]. If indeed such sign reversal can be ob-

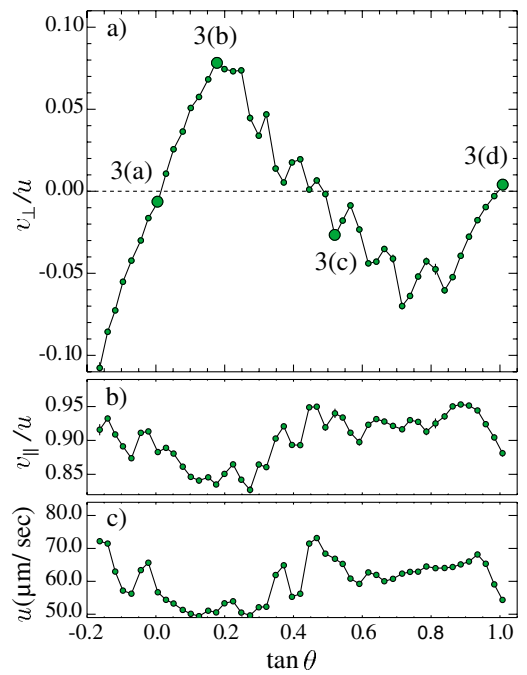


FIG. 4 (color online). (a) Variation of the mean normalized particle speed perpendicular to the externally applied force as a function of array orientation. Emphasized data points correspond to conditions in Fig. 3. (b) Mean normalized longitudinal speed. (c) Mean flow speed in the bulk for each orientation studied.

tained through simple patterning of an electronic system, the effect would be unprecedented and could have widespread applications in magnetic data retrieval.

Beyond $\tan\theta = 0.85$, trajectories become locked-in to the commensurate channeling state along the $[1\bar{1}]$ direction. The deflection returns to zero in this state when the $[1\bar{1}]$ rows align with the external force at $\tan\theta = 1$. Quantitatively indistinguishable results for $v_\perp(\theta)/u$ were obtained for particles moving with different speeds in the range $50 \mu\text{m/s} < u < 75 \mu\text{m/s}$.

While v_\perp/u is independent of u over the entire range of hopping conditions, such is not the case for the other component, v_\parallel/u . As can be seen from Figs. 4(b) and 4(c), the normalized longitudinal velocity is strongly correlated with u . Although structure in $v_\parallel(\theta)$ may reflect aspects of particles' hopping mechanisms, much as the magneto-resistance does for electron transport, it is masked in the available data by variations in u .

The $[10]$ and $[1\bar{1}]$ locked-in states are characterized by the positive slope they induce in $v_\perp(\theta)/u$. That other, smaller features also correspond to locked-in states becomes apparent in another representation of the data. Simulations [2] have demonstrated that kinetically locked-in states appear as plateaus in the θ dependence of the ratio $v_{[01]}/v_{[10]}$ of in-array speeds along the perpendicular $[01]$ and $[10]$ directions. Comparison with predictions for the circle map and related dynamic systems further suggests that the widest plateaus should be

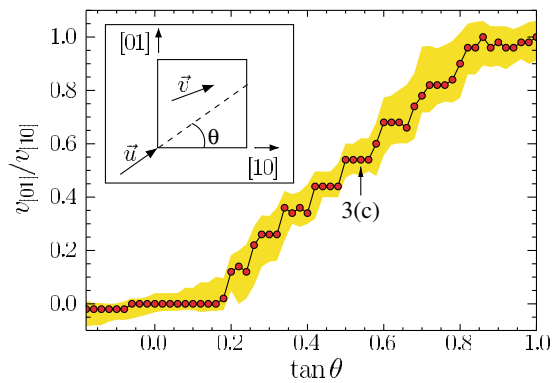


FIG. 5 (color online). Orientation dependence of particles' speeds along and normal to the $[10]$ direction reveals a series of plateaus corresponding to kinetically locked-in states. Plotted points are the most probable, or mode, values from the distribution obtained from all trajectories at each angle. Shaded regions indicate the 99% confidence interval about these values.

centered at the simplest rational values of $\tan\theta$ and that the overall hierarchy of locked-in states should take the form of a Devil's staircase with increasing rotation [2,13]. The corresponding representation of our data appears in Fig. 5. As expected, the data display a series of kinetically locked-in states, with plateaus in $v_{[01]}/v_{[10]}$ corresponding to regions of positive slope in $v_{\perp}(\theta)/u$. The large plateaus around $\tan\theta = 0$ and $\tan\theta = 1$ correspond to the $[10]$ and $[1\bar{1}]$ locked-in states. However, the higher-order plateaus between $\tan\theta = 0.2$ and $\tan\theta = 0.8$ are not centered on simple rational values of $\tan\theta$. Instead, the commensurate orientations at $\tan\theta = 1/3$, $1/2$, and $2/3$ correspond to *transitions* between plateaus. Furthermore, the associated plateaus include nonchanneling states such as Fig. 3(c) which nonetheless are locked-in.

Nonchanneling transport in the plateaus of Fig. 5 suggests a previously unrecognized class of statistically locked-in states that are distinct from deterministically channeling states. Their absence from measurements on perfect atomic crystals and idealized molecular dynamics simulations suggests that they may result from quenched disorder in our optically defined potential energy landscape. The pattern of plateaus reflects symmetries in the potential energy landscape and so would not be affected by the individual potential wells' shapes [13]. Their statistical nature suggests a possible role for random thermal forcing. How disorder gives rise to the distribution of steps observed in Fig. 5 poses an outstanding challenge.

Beyond providing an experimental context in which to study the microscopic mechanisms of kinetic lock-in, the techniques introduced for this study also constitute a practical method for continuously fractionating mesoscopic materials. Particles in a heterogeneous suspension that interact more strongly with optical traps will be pushed to one side by an appropriately tuned array of

traps. Particles that interact less strongly will pass through the same array undeflected. The deflected and undeflected fractions then can be collected in separate microfluidic channels and passed on to additional stages of optical traps for further stages of fractionation.

We are grateful to Franco Nori, Charles Reichhardt, Woowon Kang, and Sidney Nagel for enlightening conversations. This work was supported by the National Science Foundation through Grant No. DMR 9730189 and by the MRSEC program of the NSF through Grant No. DMR-9880595. Additional support was provided by a grant from Arrayx, Inc. The diffractive optical element used in this work was fabricated by Gabriel Spalding, Steven Sheets, and Matthew Dearing to a design computed by Eric R. Dufresne [10].

*Department of Physics, Illinois Wesleyan University, Bloomington, IL 61702.

- [1] O. Pierre-Louis and M. I. Haftel, Phys. Rev. Lett. **87**, 048701 (2001).
- [2] C. Reichhardt and F. Nori, Phys. Rev. Lett. **82**, 414 (1999).
- [3] M. Baert, V.V. Metlushko, R. Jonckheere, V.V. Moshchalkov, and Y. Bruynseraede, Phys. Rev. Lett. **74**, 3269 (1995); K. Harada, O. Kamimura, H. Kasai, T. Matsuda, A. Tonomura, and V.V. Moshchalkov, Science **274**, 1167 (1996); J.I. Martín, M. Vélez, J. Nogués, and I.K. Schuller, Phys. Rev. Lett. **79**, 1929 (1997); D.J. Morgan and J.B. Ketterson, Phys. Rev. Lett. **80**, 3614 (1998).
- [4] K.D. Fisher, D. Stroud, and L. Janin, Phys. Rev. B **60**, 15 371 (1999); V.I. Marconi and D. Domínguez, Phys. Rev. B **63**, 174509 (2001).
- [5] J. Wiersig and K.-H. Ahn, Phys. Rev. Lett. **87**, 026803 (2001).
- [6] B.J. Ackerson and A.H. Chowdhury, Faraday Discuss. Chem. Soc. **83**, 1 (1987); M.M. Burns, J.-M. Fournier, and J.A. Golovchenko, Science **249**, 749 (1990); K. Loudiyi and B.J. Ackerson, Physica (Amsterdam) **184A**, 1 (1992); Q.-H. Wei, C. Bechinger, D. Rudhardt, and P. Leiderer, Phys. Rev. Lett. **81**, 2606 (1998).
- [7] S.H. Behrens and D.G. Grier, Phys. Rev. E **64**, 050401 (2001); J. Chem. Phys. **115**, 6716 (2001).
- [8] J.C. Crocker and D.G. Grier, J. Colloid Interface Sci. **179**, 298 (1996).
- [9] E.R. Dufresne and D.G. Grier, Rev. Sci. Instrum. **69**, 1974 (1998).
- [10] E.R. Dufresne, G.C. Spalding, M.T. Dearing, S.A. Sheets, and D.G. Grier, Rev. Sci. Instrum. **72**, 1810 (2001).
- [11] A. Ashkin, J.M. Dziedzic, J.E. Bjorkholm, and S. Chu, Opt. Lett. **11**, 288 (1986).
- [12] E.R. Dufresne, T.M. Squires, M.P. Brenner, and D.G. Grier, Phys. Rev. Lett. **85**, 3317 (2000).
- [13] E. Ott, *Chaos in Dynamical Systems* (Cambridge University Press, New York, 1993).